

Investigation of Methyl Decanoate Combustion in an Optical Direct-Injection Diesel Engine

A. S. (Ed) Cheng*,† Cosmin E. Dumitrescu,‡,§ and Charles J. Mueller‡

†School of Engineering, San Francisco State University, 1600 Holloway Avenue, San Francisco, California 94132, United States

‡Combustion Research Facility, Sandia National Laboratories, 7011 East Avenue, Livermore, California 94550, United States

ABSTRACT: An optically accessible heavy-duty diesel engine was used to investigate the impact of methyl decanoate (MD) on combustion and emissions. Specific goals of the study were to produce experimental data for validating engine combustion models using MD (a biodiesel surrogate), as well as to determine if MD could enable soot-free leaner-lifted flame combustion (LLFC), a mode of mixing-controlled combustion associated with equivalence ratios below approximately 2. An ultralow sulfur diesel certification fuel (CF) was used as the baseline fuel, and experiments were conducted at two fuel-injection pressures with three levels of charge-gas dilution; start of combustion and duration of fuel injection were held constant. In addition to conventional pressure-based and engine-out emissions measurements, exhaust laser-induced incandescence, in-cylinder natural luminosity, and in-cylinder chemiluminescence diagnostics were used to provide detailed insight into combustion processes. Results indicate that MD effectively eliminated soot emissions but that soot formation still occurred in-cylinder, with equivalence ratios at the flame lift-off length in excess of approximately 3. Nevertheless, the oxygen content of MD sufficiently limited soot formation and promoted soot oxidation such that very little soot remained at exhaust-valve open. Nitrogen oxides (NO_x) emissions for MD relative to CF showed different trends depending on fuel-injection pressure, with distinct fuel effects influencing NO_x formation depending on engine operating condition. Hydrocarbon (HC) and CO emissions were higher for MD compared to CF and corresponded to lower fuel-conversion and combustion efficiencies. These differences were attributed to the lower-load conditions of MD, resulting from its lower energy density and the need to limit fuel-injection duration to obtain valid lift-off length measurements.

1. INTRODUCTION

Diesel (compression-ignition) engines offer higher fuel-conversion efficiencies compared to their gasoline-fueled, spark-ignition counterparts. Diesel engines can thus provide benefits in terms of limiting CO_2 emissions and global warming, as well as promote energy security in countries that are net importers of petroleum. The conventional diesel mixing-controlled combustion mode presents challenges with regard to the formation of nitrogen oxides (NO_x) and soot, a component of exhaust particulate matter (PM). Advanced combustion strategies such as homogeneous charge compression-ignition (HCCI) and others involving more-premixed, low-temperature combustion (LTC) can significantly reduce NO_x and PM emissions. Pickett et al. have demonstrated that, even during mixing-controlled combustion, a combustion mode known as leaner lifted-flame combustion (LLFC) can eliminate in-cylinder soot formation when equivalence ratios are less than approximately 2.^{1,2} If applied using traditional diesel fuels, however, this strategy is typically only successful at low- to moderate-load engine operating conditions.³

Nontraditional diesel fuels offer a means to potentially limit NO_x and PM emissions across a much wider range of engine operating conditions. For example, because leaner combustion produces lower levels of soot, oxygenated fuels are known to be highly effective in reducing PM emissions. The most commonly used oxygenated diesel fuel at present is biodiesel, a sulfur-free, renewable fuel that consists of monoalkyl esters of long-chain fatty acids derived from vegetable oils or animal fats.

Studies of biodiesel and biodiesel-component combustion include both experimental work and computational modeling. On the modeling side, researchers have sought a suitable single-component surrogate for biodiesel with a chemical kinetic mechanism having manageable complexity. Methyl butanoate ($\text{C}_5\text{H}_{10}\text{O}_2$, CAS Registry No. 623-42-7) was investigated as a potential biodiesel surrogate⁴ but was found to be a poor match to biodiesel in terms of combustion and emissions behavior.^{5–8} More recently, chemical kinetic mechanisms for methyl decanoate ($\text{C}_{11}\text{H}_{22}\text{O}_2$, CAS Registry No. 110-42-9) have produced results that better match biodiesel combustion.^{8–12} In addition, its cloud point and oxidative stability have been shown to be better than those of other biodiesel components.¹³ Several fundamental combustion experiments have been carried out using methyl decanoate in shock tubes and with bench-scale reactors.^{11,14–17} Szybist et al. have also conducted engine experiments using methyl decanoate, premixed, in a CFR octane-rating engine.¹⁸ However, to date, the authors are only aware of one study that has carried out methyl decanoate experiments in a direct-injection (DI) diesel engine. In that study, Wang et al. compared emissions from an engine fueled with soy-derived biodiesel, neat methyl decanoate, and 65% (by mass) methyl decanoate in balance *n*-heptane.²⁰ Emissions of NO_x , smoke, CO, and hydrocarbons (HC) were found to be very similar across the three test fuels, for intake-O₂ mole

Received: August 29, 2014

Revised: November 21, 2014

Published: November 24, 2014



fractions higher than 16%. No comparisons were made to emissions from a baseline diesel or other pure-hydrocarbon fuel. Very recently, Manin et al. have published their results comparing methyl decanoate to *n*-dodecane ($C_{12}H_{24}$) and four oxygenated blends of tripropylene glycol monomethyl ether ($C_{10}H_{22}O_4$), using a constant-volume combustion vessel.²¹ Methyl decanoate was found to produce a longer flame lift-off length relative to *n*-dodecane, an effect attributed to a different spatial distribution of stoichiometric mixtures in the flow field. The longer flame lift-off length resulted in leaner combustion and lower soot mass.

The objective of the current study is to investigate in detail the combustion and emissions performance of methyl decanoate using an optical, DI diesel engine that enables in-cylinder imaging of combustion phenomena. Specific goals include identifying the extent to which methyl decanoate can enable sustained, soot-free LLFC by reducing the equivalence ratios in combustion regions where soot formation would otherwise occur. In addition, the experiments seek to generate experimental data that can be used to assess and improve engine simulations of biodiesel combustion based on methyl decanoate mechanisms. Experimental data were collected for methyl decanoate as well as a baseline hydrocarbon diesel fuel. Diagnostics include conventional heat-release analysis, engine-out emissions, and high-speed in-cylinder imaging of both natural luminosity and OH chemiluminescence.

2. EXPERIMENTAL SETUP AND PROCEDURES

Engine and Fuel System. Experiments were performed in a single-cylinder version of a heavy-duty engine modified to provide optical access to the combustion chamber. A schematic and specifications of the engine are provided in Figure 1 and Table 1, respectively. The major differences between the optical engine and a comparable production engine relate to the piston bowl, which has a

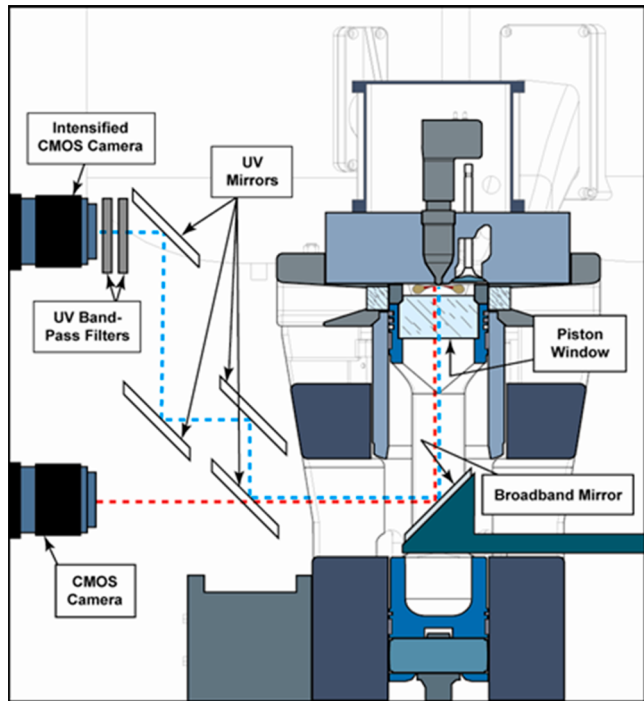


Figure 1. Schematic of optical engine. The intensified camera is used for chemiluminescence imaging; the nonintensified camera is used for natural luminosity imaging.

Table 1. Optical Engine Specifications

research engine type	single-cylinder
cycle	4-stroke CIDI
valves per cylinder	4
bore	125 mm
stroke	140 mm
intake valve open ^a	32° BTDC exhaust
intake valve close ^a	153° BTDC comp
exhaust valve open ^a	116° ATDC comp
exhaust valve closed ^a	11° ATDC exhaust
connecting-rod length	225 mm
piston-pin offset	none
piston-bowl diameter	90 mm
piston-bowl depth	16.4 mm
squish height	1.5 mm
swirl ratio ^b	0.59
displacement	1.72 L
compression ratio (geometric)	12.3:1

^aAll valve timings are for 0.03 mm lift. ^bMeasured at the Caterpillar Technical Center using an AVL swirl meter.

flat bottom, vertical walls, and a larger land above the top compression ring. The larger top-ring land allows optical access through a notch in the bowl rim and prevents the rings from riding over the cylinder-wall windows. These differences lead to a lower geometric compression ratio (CR) of 12.3:1 for the optical engine versus ~16:1 for the comparable production engine. To compensate for the lower CR in the optical-engine experiments, the intake temperature and pressure are elevated to closely match the conditions in the production engine over the crank-angle range during which combustion occurs.²²

During the experiments, the engine was skip-fired with one fired cycle followed by four motored cycles (i.e., one fired cycle every five cycles). This approach was used to reduce the rate of soot accumulation on the combustion-chamber windows and to lower the risk of window failure due to the thermal and mechanical stresses generated when switching between motored and fired operation.³ Using this approach, the residual exhaust gas that remains trapped in the combustion chamber after a fired cycle is replaced with fresh intake charge—i.e., air, nitrogen (N_2), and/or carbon dioxide (CO_2)—during the subsequent motored cycles. The heat rejection from the combustion chamber to the coolant is lower due to the skip-fired operation. Thus, an engine-coolant heater is used to maintain an engine temperature comparable to that of an engine operating in a continuously fired mode.

Fuel delivery was accomplished using a high-pressure common-rail fuel-injection system, comprised of a diaphragm pump (Newport Scientific, model 46-16060) and a near-production Caterpillar electronically actuated solenoid-operated fuel injector. The fuel-wetted internals of the pump are fabricated from stainless steel, Kalrez, or Teflon, making the system suitable for handling a wide range of conventional and unconventional fuels having high corrosivities, low viscosities, or other properties that can cause conventional piston-type pumps to fail.

Fuel injector specifications are provided in Table 2. A two-hole injector tip was used to isolate as much as possible spray mixing,

Table 2. Fuel Injector Specifications

injector type	Cat CR350
injector tip style	Mini-sac
number of injector orifices	2
orifice diameter (nom)	110 μ m
orifice length-to-diameter ratio	8
hydro-erosion	20 \pm 2%
included spray angle	140°

vaporization, and combustion from interactions with neighboring jets. X-ray tomography was used to confirm the orifice diameter, length-to-diameter ratio, and included spray angle. Figure 2 presents typical

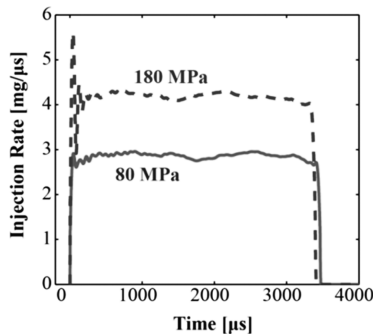


Figure 2. Injection rate profiles (per injector orifice) for 80- and 180-MPa injection pressures and an indicated duration of injection of 3500 μs .

injection-rate profiles for the two-hole tip at injection pressures of 180 and 80 MPa, as measured using a momentum-based rate-of-injection meter developed at Sandia.²³

A flush-mounted, water-cooled pressure transducer (AVL model QC32C) was used to measure cylinder-pressure every 0.5 CAD. Gas analyzers (California Analytical Instruments, Series 600) measured CO, CO₂, O₂, NO_x, and HC emissions. Soot-particle emissions were quantified using both a smoke meter (AVL model 415S) and a prototype exhaust laser-induced incandescence (LII) instrument.²⁴ Reference 25 describes in detail the procedures used for cylinder pressure data acquisition and how skip-fired exhaust-gas measurements were converted to values similar to those that would be obtained if the engine was operated in a continuously fired mode. References 3 and 22 provide further details of the experimental setup and procedures.

Test Fuels and Engine-Operating Conditions. The test fuel investigated was methyl decanoate (MD), a single-component oxygenated fuel having the chemical formula C₁₁H₂₂O₂ and molecular structure shown in Figure 3. MD has an oxygen content of 17.2% by



Figure 3. Molecular structure of methyl decanoate (C₁₁H₂₂O₂).

mass and can be produced from renewable feedstocks. Selected properties of MD are presented in Table 3. The baseline fuel was an

Table 3. Selected Properties of Methyl Decanoate Test Fuel

parameter	value	source
cetane number	51.6	ref 13
density at 300 K	871 kg/m ³	measured
boiling point (at 1 atm)	224 °C	ref 25
kinematic viscosity at 40 °C	1.71 mm ² /s	ref 13
oxygen content	17.2 mass%	calculated
molar C/H ratio	0.5	calculated
heat of combustion	37,178 kJ/kg	ref 13

ultralow sulfur diesel (ULSD) certification fuel (CF), with properties as shown in Table 4. Because of its oxygen content, MD has a gravimetric energy density (energy per unit mass) that is 13.4% lower than the baseline CF.

Table 5 presents the engine operating parameters that were held constant during the experiments. The intake charge, cylinder liner, and head were maintained at the same temperature to minimize the

Table 4. Fuel Properties of Baseline Ultra-Low Sulfur Diesel Certification Fuel^a

parameter	ASTM method	result
specific gravity [g/mL]	D4052	0.848
cetane number	D613	43.3
distillation temperature [°C]	D86	
T10		211
T50		253
T90		310
carbon [mass %]	DS291	87.04
hydrogen [mass %]	DS291	13.03
molar C/H ratio		0.561
sulfur [ppm]	DS453	14.4
aromatics (by SFC)	DS186	
one ring [mass %]		20.7
two or more rings [mass %]		9.0
total [mass %]		29.7
net heat of combustion [MJ/kg]	D240	42.9
kinematic viscosity @ 40 °C [mm ² /s]	D445	2.3

^aFrom Tables 1 and 8 of Ref 27.

Table 5. Constant Engine Operating Parameters

speed	1500 rpm
intake manifold pressure	250 kPa
intake manifold temperature	95.0 °C
coolant temperature	95 °C
injection duration (indicated)	3640 μs
start of combustion	-5 CAD ATDC

uncertainty in charge-gas temperature at the beginning of the compression stroke due to heat transfer among these elements of the system. The start of injection (SOI) was adjusted to maintain a constant start of combustion (SOC) timing.

Three dilution levels were studied in this work. Because the skip-fired operating mode that was employed in these experiments affects the exhaust-gas composition, real exhaust-gas recirculation (EGR) was not used to achieve these dilution levels. Instead, the mole fraction of oxygen in the intake mixture (X_{O_2}) was varied by adding N₂ and CO₂ to the dry intake air. Table 6 shows the mole fractions of O₂, N₂, CO₂,

Table 6. Species Mole Fractions (X) and Densities (ρ) of the Studied Charge-Gas Mixtures

parameter	21-mol % O ₂ (dry air)	18-mol % O ₂	16-mol % O ₂
X _{O₂} [mol %]	20.947	18.000	16.000
X _{N₂} [mol %]	78.084	80.899	82.811
X _{CO₂} [mol %]	0.035	0.298	0.476
X _{Ar} [mol %]	0.934	0.803	0.713
ρ at -10 CAD ATDC [kg/m ³]	26.0	25.9	25.8

and argon (Ar) in each intake mixture, as well as the intake-mixture densities (ρ) at -10 CAD ATDC. The experiment was designed such that the specific heat (C_p), temperature (T), and pressure (p) of each charge-gas mixture were held constant at -10 CAD ATDC under motored conditions at 32.1 J/mol/K, 850 K, and 63.3 bar, respectively. This approach was used to (1) isolate the effects of X_{O_2} variation on the results (independent of C_p variation); (2) enable liquid-phase fuel penetration lengths measured under the same in-cylinder thermodynamic conditions (but without appreciable heat release at 2 mol % X_{O₂}, see refs 18 and 19) to be applicable to the present study; and (3)

reduce the rate of consumption of bottled CO₂ during the experiments.

Experiments were performed at two fuel-injection pressures (180 and 80 MPa). Injection timing and injection duration were selected to obtain predominantly mixing-controlled combustion (i.e., minimum premixed burn) and accurate optical measurements over the duration of heat release. Injection timing was adjusted such that SOC was maintained at -5 CAD ATDC for all engine runs. Advancing SOC resulted in higher premixed burn fractions, while delaying SOC adversely affected the efficiency and emissions. The precise determination of SOC is made based upon the crank angle where the high-temperature heat release (HTHR) first becomes positive after start of injection (SOI). Depending on operating condition, SOI ranged from -7.7 to -9.6 CAD ATDC for CF and from -7.2 to -9.1 CAD ATDC for MD. The average difference corresponds to a 0.45-CAD shorter ignition delay for the higher cetane number MD.

As shown in Table 5, the duration of injection (DOI) was kept constant for all engine runs. Because of the energy density difference between the two test fuels, engine runs with MD were at lower loads relative to their CF counterparts, as shown in Table 7. In conventional

Table 7. Injection Pressures and Engine Loads

injection pressures	80 MPa, 180 MPa
gIMEP ^a (at injection pressure) for certification fuel	170 kPa (at 80 MPa), 290 kPa (at 180 MPa)
gIMEP (at injection pressure) for methyl decanoate	123 kPa (at 80 MPa), 212 kPa (at 180 MPa)

^agIMEP = gross-indicated mean-effective pressure.

fuel-effects studies that measure engine-out emissions, an effort is typically made to maintain engine load at a constant value. However, increasing the DOI for MD to match the CF load was not possible without obstructing the optical measurement of flame lift-off length (discussed in more detail below). Reducing the DOI for CF to match the MD load would affect the relative durations of the premixed and mixing-controlled combustion modes. These trade-offs, combined with a desire to focus on fundamental combustion phenomena and in-cylinder processes, led to the use of constant DOI rather than constant engine load.

The engine was skip-fired at 1500 rpm for a minimum of 180 fired cycles per engine run. To ensure good data repeatability, at least three runs (540 engine cycles) of pressure-based data were recorded at each operating condition, generally taken on different days during no fewer than three separate optical-engine runs.

Optical Diagnostics. Two high-speed cameras were used to simultaneously record natural luminosity and OH chemiluminescence during the first 10 fired cycles of each engine run.

Natural luminosity (NL) refers to the broadband light emitted by the combustion process during a fired cycle. This luminosity arises from both soot incandescence and chemiluminescence, but the contribution from soot incandescence has been shown to be 3–5 orders of magnitude higher than that from chemiluminescence during mixing-controlled combustion.²⁸ NL images can thus be used to indicate the locations of high-temperature soot particles.²⁹ An NL image was collected every 0.5 CAD using a high-speed CMOS camera (Vision Research, Model Phantom v7.3) fitted with a 35 mm Nikon lens. The NL signal included wavelengths in the range of 380–1000 nm. As shown in Figure 1, the combustion chamber is visualized from below through the fused-silica piston window using a 45° mirror. The field of view is 104 mm × 96 mm with a spatial resolution of 0.5 mm/pixel.

Spatially integrated natural luminosity (SINL) was determined at each CAD by summing the intensities of all pixels, corrected for image exposure and aperture setting:

$$\text{SINL(CAD)} = \frac{f_s^2}{t_{\text{exp}} \text{SINL}_{\text{max}}} \sum_{y=1}^m \sum_{x=1}^n \text{NL}(x, y, \text{CAD}) \quad (1)$$

In eq 1, n and m are the number of pixels in the x - and y -directions, respectively; f_s is the lens f-stop; and t_{exp} is the image exposure duration. SINL_{max} is the signal that would be measured if all pixels within the piston bowl were saturated when the lens aperture and exposure time were set to their minimum values (i.e., $f_s = 16$ and $t_{\text{exp}} = 1.0 \mu\text{s}$). SINL values provide a time-resolved, quantitative measure of high-temperature soot that can be compared between different engine runs. Further details of the NL data-acquisition procedure can be found in ref 3.

Chemiluminescence (CL) signals from electronically excited hydroxyl radicals (OH) at 308 ± 10 nm were used to determine the flame lift-off length (H). H is defined as the axial distance between the fuel-injector orifice exit and the position where the standing premixed autoignition zone stabilizes during mixing-controlled combustion.^{1,30,31}

A CL image was collected every 1.0 CAD using an intensified CMOS camera (Vision Research, Model Phantom v7.1) and a Nikon 105 mm ultraviolet (UV) lens. A sequence of 96 mm × 96 mm images with a spatial resolution of 0.25 mm/pixel was captured during each fired cycle. CL images were analyzed following the procedure described in ref 3. H for each fuel jet was determined using

$$H = \frac{H_{2d} - r_{\text{inj}}}{\sin(\theta_i/2)} \quad (2)$$

where H_{2d} is the lift-off length in the plane of the image, defined by the position along the jet axis where the gradient of the base-10 logarithm of the CL intensity profile reaches its maximum value. r_{inj} is the radial offset of the injector orifice from the injector-tip axis, and θ_i is the included spray angle. For this engine and injector configuration, it has been previously observed that H measurements are unreliable beyond a maximum injection duration.³ Longer injection durations lead to CL interacting with the bowl rim and being redirected back toward the bore axis, erroneously shortening measured H values. In this study, the engine operating conditions of Table 5 maintained a relatively constant value of H over the duration of mixing-controlled combustion. References 3 and 32 provide additional details of the optical equipment and analysis procedures used for the H measurements.

The equivalence ratio at the flame lift-off length, $\phi(H)$, has been shown to correlate with in-cylinder soot levels, with a critical value of $\phi(H) \cong 2$ below which soot is not formed.¹ In this study, $\phi(H)$ is calculated using Naber and Siebers' relationship,³³ which quantifies the cross-sectional average equivalence ratio along the axis of a nonreacting, isothermal jet:

$$\phi(x) = \frac{2(A/F)_{\text{st}}}{\sqrt{1 + 16\left(\frac{x}{x^+}\right)^2} - 1} \quad (3)$$

$$x^+ = \sqrt{\frac{\rho_F}{\rho_A}} \left\{ \frac{d_0 \sqrt{C_a}}{c \left[\left(\frac{\rho_A}{\rho_F} \right)^{0.19} - 0.0043 \sqrt{\frac{\rho_F}{\rho_A}} \right]} \right\} \quad (4)$$

In eq 3, $(A/F)_{\text{st}}$ is the stoichiometric ambient-gas to fuel mass ratio, x^+ is a characteristic length scale, ρ_A and ρ_F are the ambient-gas and fuel densities, respectively, d_0 is the injector orifice diameter, and c and C_a values were taken from ref 34. In eq 4, measured values of H and bulk-gas-average density ρ , calculated based on the trapped charge mass and piston position, are used for x^+ and ρ_A , respectively. In applying eqs 3 and 4 to determine $\phi(x)$, it was assumed that $\phi(x)$ changes on the same time scale as H and ρ , and that the ϕ -field for the two-hole injector tip used in this work is similar to the single, free jet used to develop the equation. Recently, Pickett et al. suggested that $\phi(x)$ calculated with Naber and Siebers' model may be more representative of the jet-centerline than the cross-sectional-average equivalence ratio,³⁵ and thus the actual cross-sectional average equivalence ratio may be lower. However, spatially integrated NL

measurements have supported the assumption that eq 3 can be used to estimate $\phi(H)$, because significant NL appears only for values of $\phi(H)$ greater than 2.³⁶ These observations are similar to those made in the constant-volume combustion vessel used to develop eqs 3 and 4.¹

H measurements present inherent jet-to-jet and cycle-to-cycle variations on the order of 30% of the mean value,^{1,3,32,37} corresponding to variations in $\phi(H)$ up to twice its instantaneous mean value. This issue is addressed by defining a mean value at each crank angle during the injection process, $\langle H(\text{CAD}) \rangle$:

$$\langle H(\text{CAD}) \rangle = \frac{1}{n_{\text{cycle}} n_{\text{jets}}} \sum_{c=1}^{n_{\text{cycle}}} \sum_{j=1}^{n_{\text{jets}}} H(j, c, \text{CAD}) \quad (5)$$

In eq 5, $H(j, c, \text{CAD})$ represents the lift-off length measurement from a single jet and cycle, at a specific crank-angle degree; n_{jets} is the number of injector orifices, and n_{cycle} is the number of engine cycles imaged. For notational simplicity, $\langle H(\text{CAD}) \rangle$ will be referred to as H in the rest of this paper.

Averaging the equivalence ratio at the lift-off length over the total number of imaged cycles and injector jets can hide jet-to-jet variations, especially for operating conditions where $\phi(H)$ is close to the nonsooting limit ($\phi(H) \cong 2$). In this case, one soot-producing jet ($\phi(H) > 2$) may be responsible for all of the soot production if $\phi(H)$ for all other jets is lower than the soot limit. However, no large cyclic variations in NL were observed from one jet to another, and there were no outliers in soot emissions measurements when correlated to $\phi(H)$.

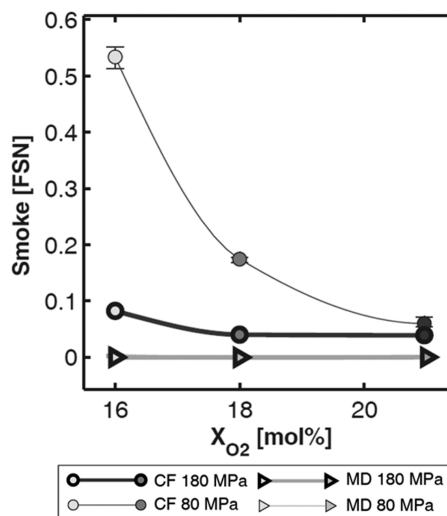


Figure 4. Filter smoke number (FSN) as a function of intake-O₂ mole fraction. FSN values for MD at both injection pressures are effectively zero and thus appear as a single trendline.

3. RESULTS AND DISCUSSION

Soot. Figure 4 presents filter smoke numbers (FSN; measured with the AVL smoke meter) as a function of X_{O_2} for the two test fuels at the 180- and 80-MPa injection pressures. FSN values for MD at both injection pressures are effectively zero and thus appear as a single trendline. As will be the case with similar figures presented in this paper, data points in Figure 4 represent averages over at least three replicate measurements at the same test condition; error bars denote minimum and maximum observed values.

Exhaust-LII measurements are presented in Figure 5. For MD, measured LII values are effectively zero with the exception

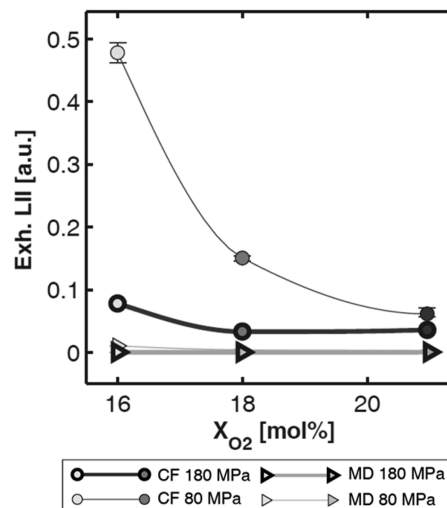


Figure 5. Exhaust laser-induced incandescence measurements (arbitrary units) as a function of intake-O₂ mole fraction.

of the low-pressure injection, 16%- X_{O_2} case. An absolute calibration of the exhaust-LII measurements to soot volume fraction was not undertaken in the preparation of Figure 5, but comparisons of relative signal levels between data points are valid.

Figures 4 and 5 show that, for the engine operating conditions of this study, CF produces significant soot emissions that are effectively eliminated when the engine is fueled with MD. Both measures of exhaust soot are in excellent agreement with each other and are consistent with the well-known effect of biodiesel on soot, with percent reductions that scale with and are more significant than the mass percent of fuel oxygen.^{32,38–40} In particular, the data indicate that MD dramatically reduces engine-out soot at the lower-injection pressure, higher-dilution (higher-EGR) cases for which soot emissions are more problematic.

Soot emissions result from complex in-cylinder processes of soot formation and subsequent oxidation. Therefore, exhaust measurements cannot provide direct insight into in-cylinder soot concentrations. To better understand the in-cylinder processes, collected NL images and calculated SINL values from eq 1 can be evaluated. NL images from the different engine runs reveal observable soot incandescence in *all* cases, even those for MD for which FSN and exhaust-LII values were negligible. NL images for CF and MD at 18% X_{O_2} and 180-MPa fuel-injection pressure are shown in Figure 6 and provide a good representation of the images collected at other dilution levels and at the lower fuel-injection pressure. Because of different image acquisition parameters (exposure time and aperture setting), the relative intensities of the CF and MD images should not be directly compared.

Figure 6 reveals that soot incandescence first appears slightly downstream of the lift-off length and continues in the radial direction until it is redirected by the piston-bowl rim. For the MD runs, NL tapers off gradually during heat release, while for CF, NL drops more suddenly and later in the cycle. The timeline and relative magnitudes of in-cylinder NL can be viewed quantitatively in Figures 7 and 8, which present CAD-

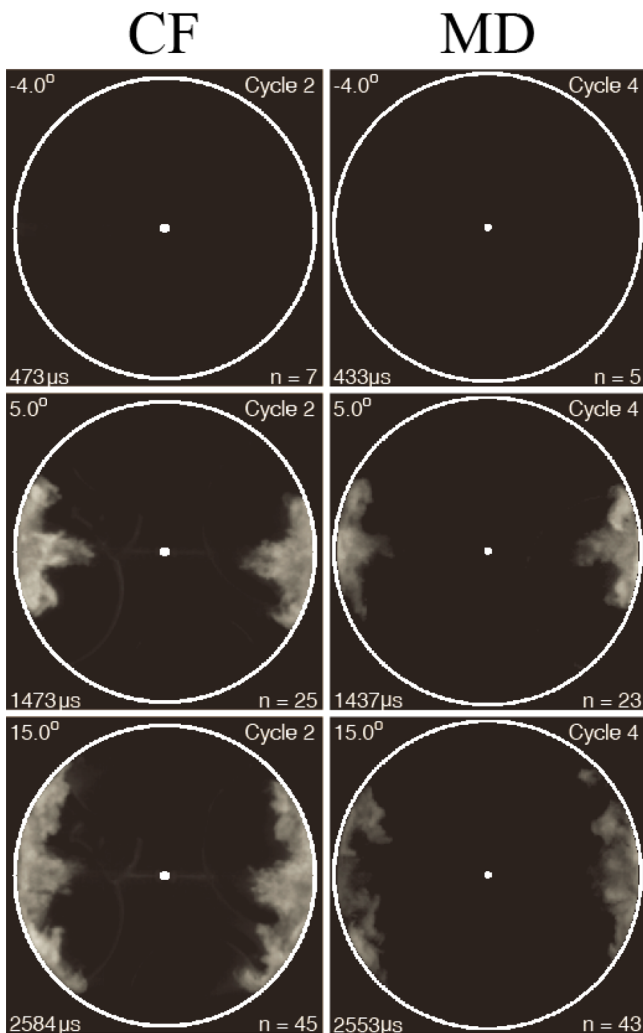


Figure 6. NL images for CF and MD at 18% X_{O_2} and 180-MPa fuel-injection pressure. The dot in the center of each image and the circular border denote the injector tip and piston bowl-rim, respectively. Because of different image-acquisition parameters, the relative intensities of the CF and MD images should not be compared. Numerical values shown on the images are (clockwise from top-left): CAD after TDC, fired-cycle number, image number, and time after start of injection.

resolved SINL and apparent heat release rate (AHRR) for the 180- and 80-MPa injection pressure cases, respectively. As these figures show, the natural luminosity for MD is much lower than for the corresponding CF runs. For MD, the shape of the SINL curve can be interpreted as an initial rise as soot particles form (and reach high temperature), followed by a gradual reduction as soot oxidation overtakes/replaces soot formation. Much of the in-cylinder NL disappears before or around the end of the main heat release at $\sim 20\text{--}30$ CAD ATDC. For CF, the shapes of the SINL curves are noticeably different. Much more and/or hotter soot is produced in-cylinder, and the sharp drop-off in SINL that occurs later in the expansion stroke ($\sim 35\text{--}45$ CAD ATDC) is consistent with rapidly cooling soot particles that are no longer luminous (rather than no longer present). It should be noted that the irregular peaks in the CF SINL curves are apparently associated with soot moving into and out of the squish volume (which is blocked from view by the piston-

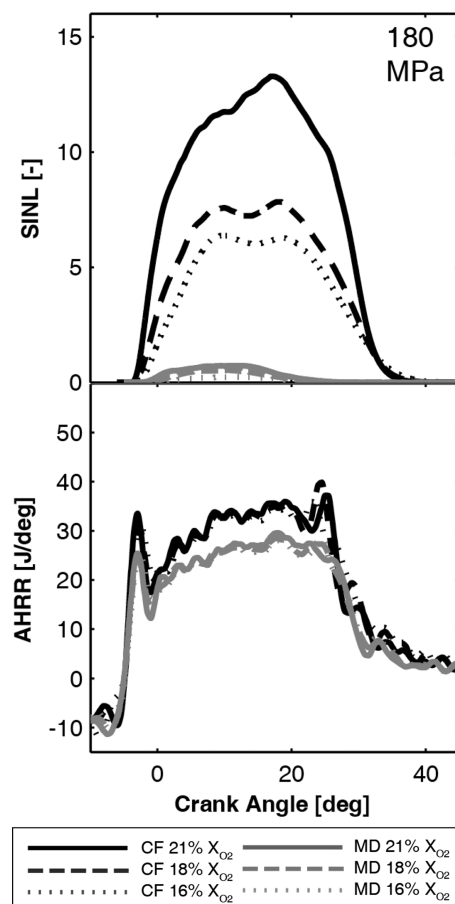


Figure 7. Spatially integrated natural luminosity (SINL) and apparent heat release rate (AHRR) for 180-MPa injection pressure cases.

window retainer ring), rather than actual in-cylinder NL fluctuations.

Measured lift-off lengths (H) for the 180- and 80-MPa injection pressure cases are shown in Figure 9. These data are obtained from the CL images and eq 2. Representative CL images for CF and MD at 18% X_{O_2} and 180-MPa fuel-injection pressure are shown in Figure 10. As was the case for Figure 6, the relative intensities of the CF and MD images should not be directly compared, as CL image-acquisition parameters (exposure time, aperture setting, and intensifier gain) were varied from run to run to obtain the best images.

The fundamental physical process that establishes the lift-off length is not conclusively understood. One explanation is that the lift-off length occurs at the downstream distance to which a parcel of fuel travels during its ignition-delay time under the given in-cylinder ambient and mixing conditions. Another is that the lift-off length is established where the local upstream flame-propagation speed is balanced by the local flow velocity that is convecting the mixture downstream. Regardless, the lift-off length data provide additional insight into factors affecting soot formation for each of the fuels, and lift-off lengths are expectedly larger for the higher injection pressure (higher injection velocity) cases.

For a given fuel at a given injection pressure, lift-off length increases with increasing dilution (decreasing X_{O_2}). This effect, which has also been shown by Siebers et al.,⁴¹ is consistent with the idea that additional charge-gas entrainment is necessary to reach comparable (and combustible) mixture stoichiometries at

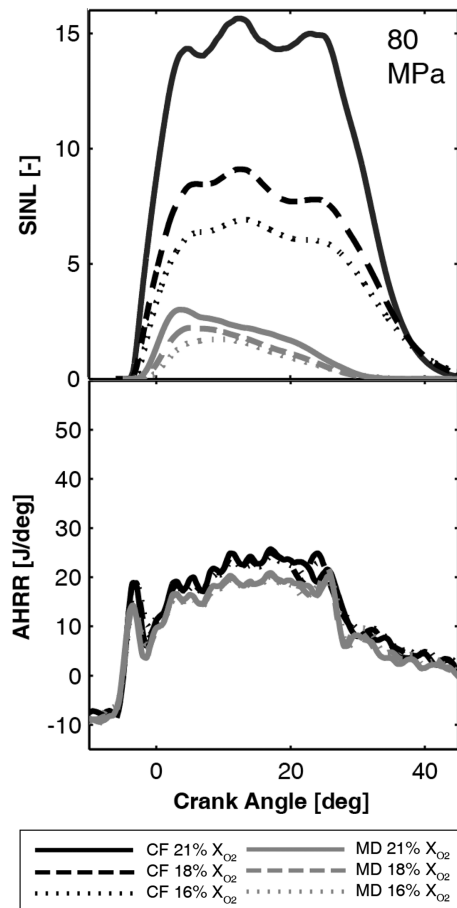


Figure 8. Spatially integrated natural luminosity (SINL) and apparent heat release rate (AHRR) for 80-MPa injection-pressure cases.

the lift-off length, as charge-gas oxygen levels decrease. Upon the basis of this reasoning, one might expect lift-off lengths to be shorter for the oxygenated and higher-cetane MD fuel, yet they are similar for both fuels at a given injection pressure and dilution level. Longer than expected lift-off lengths for MD could be due to the fuel's lower load engine operating conditions, which result in lower in-cylinder temperatures. In addition, Manin et al. have recently reported that fuel oxygen content increased lift-off lengths for fuels with similar ignition delays.²¹ They suggest the effect may be due to the fuel-bound oxygen shifting the radial location of stoichiometric mixtures closer to the jet axis, where flow velocities are higher. If the flame stabilizes at a location where flame-propagation speeds match flow velocities (and the flame-propagation speeds of CF and MD are comparable), the result would be a longer than expected lift-off length for MD because flow velocities also decrease with distance from the injector tip.

While significant fuel effects on lift-off lengths were not observed, the calculated equivalence ratio at the lift-off length, $\phi(H)$, was notably lower for MD relative to the corresponding CF cases. These data are shown in Figure 11; $\phi(H)$ values averaged over CAD are shown in Figure 12. With comparable fuel densities and comparable lift-off lengths, $\phi(H)$ is governed primarily by the stoichiometric ambient-gas to fuel mass ratio, $(A/F)_{st}$, which is lower for the oxygenated MD fuel. As shown in Figures 11 and 12, MD did not produce the lower than $\phi(H) \cong 2$ values associated with soot-free LLFC. However, the lower equivalence ratios at the lift-off length for MD are likely the

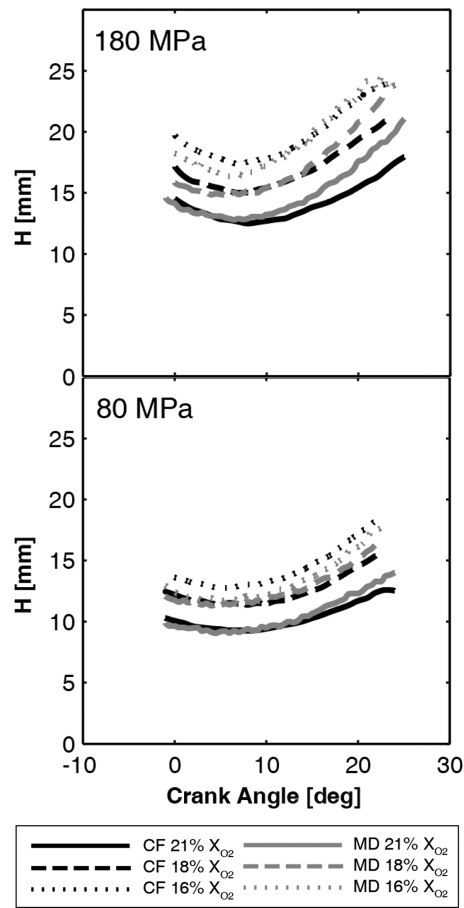


Figure 9. Lift-off length, H , as determined by OH chemiluminescence.

primary factor contributing the fuel's lower SINL and near-zero soot emissions.

When considered together, all of the measurements discussed above support the following explanations of soot formation/oxidation and emissions for the two fuels:

For CF, following the premixed burn, mixing-controlled combustion continues at a relatively constant lift-off length with local equivalence ratios high enough to generate substantial soot downstream of the autoignition zone. This soot formation occurs in the zone labeled "Products of Rich Combustion" in the conceptual image of mixing-controlled diesel combustion shown in Figure 13. The competing rates of soot formation and oxidation are such that soot concentrations remain significant throughout combustion, and also into the expansion stroke when the soot particles cool, can no longer be oxidized, and subsequently leave the engine.

For MD, mixing-controlled combustion occurs with comparable lift-off lengths to CF. However, fuel-bound oxygen significantly lowers local equivalence ratios at the lift-off length and minimizes soot formation downstream of the autoignition zone. The increased oxygen availability and lower soot concentrations are such that most particles are oxidized prior to the end of combustion, leaving very little soot to leave the engine.

The equivalence ratios shown in Figures 11 and 12 do present a seeming contradiction to the above explanations—namely, that $\phi(H)$ for MD at 80 MPa is higher than that for CF at 180 MPa, yet lower NL and soot emissions are associated with the former compared to the latter. Recall, however, that

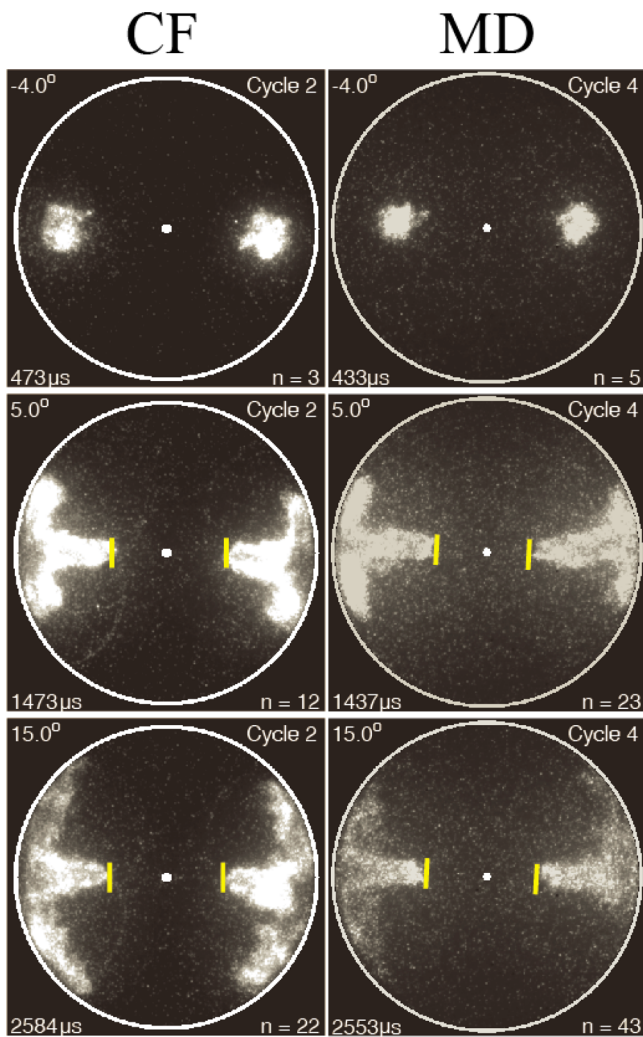


Figure 10. Sample CL images for CF and MD at 18% X_{O_2} and 180-MPa fuel-injection pressure. The images shown were collected simultaneously with the corresponding NL images in Figure 6. The dot in the center of each image and the circular border denote the injector tip and piston bowl-rim, respectively. Vertical lines on the images indicate measured H values. Because of the different image-acquisition parameters, the relative intensities of the CF and MD images should not be directly compared. Numerical values shown on the images are (clockwise from top-left): CAD after TDC, fired-cycle number, image number, and time after start of injection.

$\phi(H)$ represents the cross-sectional average equivalence ratio at the lift-off length. Although $\phi(H)$ is larger for MD at 80 MPa relative to CF at 180 MPa, local equivalence ratios for the oxygen-containing MD, along and very close to the jet axis, would be significantly lower than for CF, which contains no oxygen. In addition, the well-known impact of aromatic compounds on soot-precursor formation cannot be overlooked. Even if MD and CF were to produce comparable jet-axis equivalence ratios at the lift-off length, the presence of aromatics in the CF fuel would likely result in a higher sooting potential.

NO_x Figure 14 presents indicated specific NO_x emissions as a function of X_{O_2} for the two test fuels at the 180- and 80-MPa injection pressures. NO_x emissions for MD at both injection pressures are nearly identical and thus appear as a single trendline. The figure shows the expected effect of dilution, with

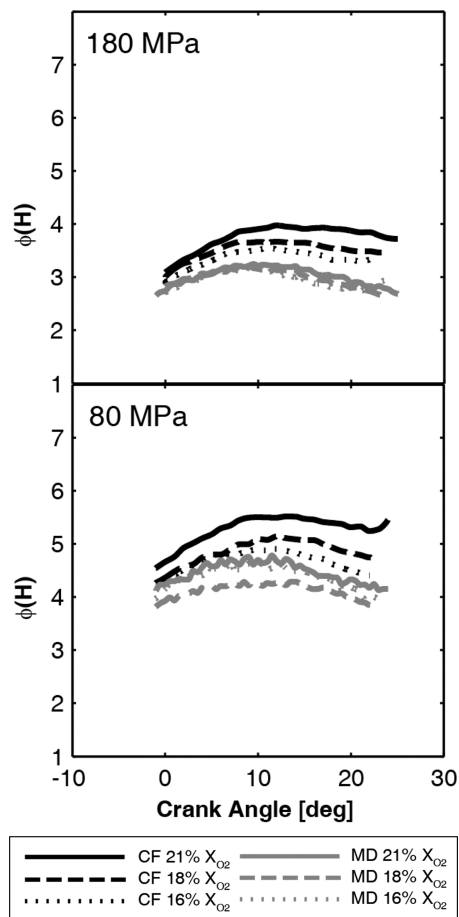


Figure 11. Equivalence ratio at the lift-off length.

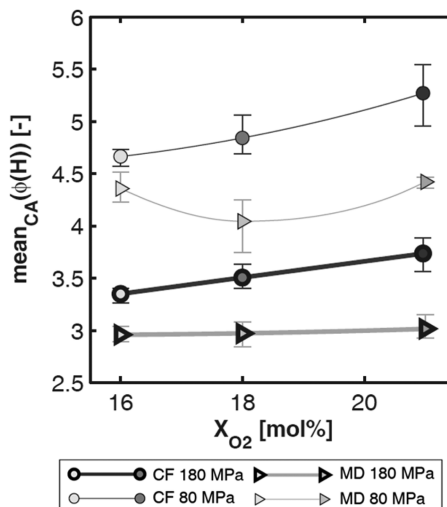


Figure 12. Average equivalence ratio at the lift-off length as a function of intake- O_2 mole fraction.

lower NO_x emissions at higher dilution (i.e., lower X_{O_2}) levels. Comparing fuels at the 180-MPa injection pressure, NO_x emissions for MD are ~14–18% lower than those of CF. However, at the lower 80-MPa injection pressure, MD NO_x emissions are comparable to or slightly higher than those of CF.

The diagnostics used in this study do not provide direct insight into in-cylinder NO_x concentrations. Thus, the specific mechanisms that produce the observed NO_x emissions trends

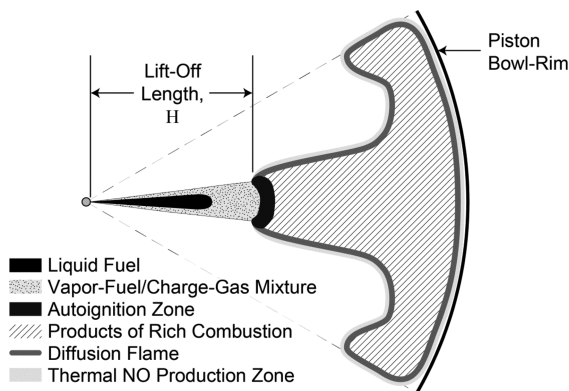


Figure 13. Conceptual image of mixing-controlled diesel combustion.

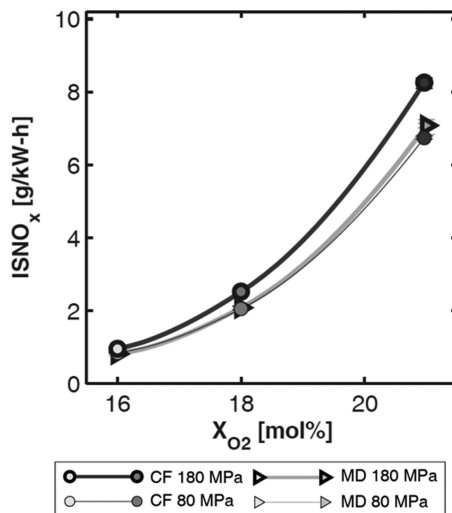


Figure 14. Indicated specific NO_x emissions as a function of intake- O_2 mole fraction. NO_x emissions for MD at both injection pressures are nearly identical and thus appear as a single trendline.

cannot be identified with certainty, but insights from other studies can be helpful. The present understanding of mixing-controlled combustion indicates that most of the NO_x formation occurs via the thermal (Zeldovich) NO_x mechanism at the periphery of the combustion zone—i.e., at the thin line labeled “Thermal NO Production Zone” in Figure 13.⁴² Because start of combustion was controlled at -5 CAD ATDC, differences in thermal NO_x production must be driven by other factors affecting in-cylinder combustion temperatures. Via a method for calculating the adiabatic flame temperature (T_{adb}) based upon C/H ratio (see Figure 15 of ref 32), T_{adb} for CF can be shown to be slightly higher than that for MD. This, combined with the higher loads (and thus higher temperatures) during CF engine operation, could explain the increased NO_x emissions for the 180-MPa injection pressure.

NO_x emissions from the 80-MPa injection pressure case are more difficult to interpret. Factors other than those presented above must have increased importance and drive MD NO_x emissions higher, relative to those for CF, even though the CF engine load is higher. Several factors that could explain higher NO_x emissions with biodiesel esters relative to hydrocarbon (i.e., nonoxygenated) fuels are discussed and evaluated in ref 32. All of these center on the methyl ester(s) (in this case MD) producing higher in-cylinder temperatures and/or longer residence times at high temperature because these changes

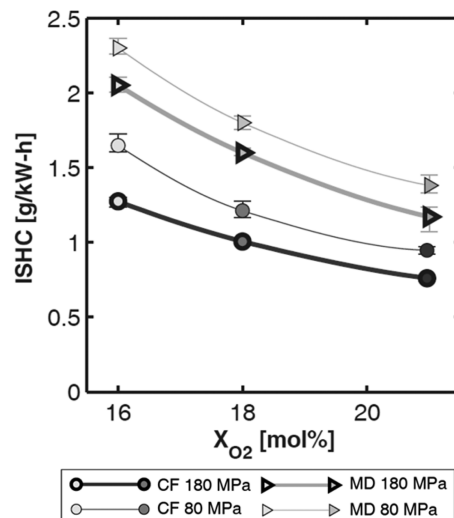


Figure 15. Indicated specific HC emissions as a function of intake- O_2 mole fraction.

will increase thermal NO_x formation. While these factors do not appear to govern NO_x emissions at the higher 180-MPa injection pressure, they may play a more significant role at the 80-MPa injection pressure where fuel atomization and mixing with charge-gas are a greater challenge. For instance, at the lower injection pressure, the fuel-bound oxygen in MD might more substantially increase regions where combustion is closer to stoichiometric (and thus higher temperature) and/or increase the availability of atomic oxygen in NO_x formation zones. Other fuel-chemistry effects, including those that may affect prompt NO_x formation, may also be important.

HC and CO. Indicated specific HC and CO emissions as a function of X_{O_2} are shown in Figures 15 and 16, respectively. HC and CO emissions decrease with decreasing charge dilution and for the higher 180-MPa injection pressure. These trends are consistent with additional oxygen availability (either due to decreased dilution or enhanced fuel/charge-gas mixing) promoting more complete oxidation. In addition, the 180-

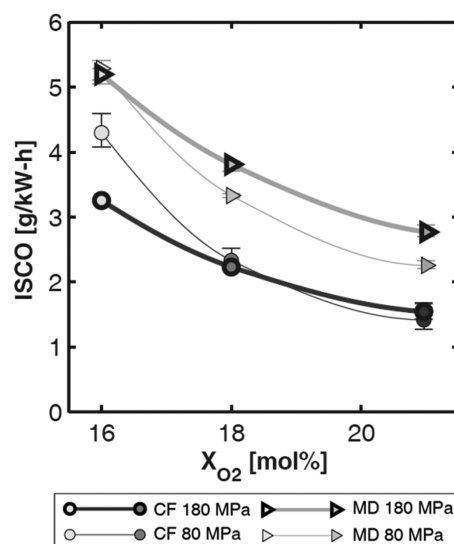


Figure 16. Indicated specific CO emissions as a function of intake- O_2 mole fraction.

MPa injection pressure case produced a more rapid (and thus closer to TDC) heat release, which would produce higher temperatures and promote HC and CO oxidation. In terms of fuel effects, indicated specific emissions of both HC and CO are higher for MD relative to the corresponding CF cases. While MD is an oxygen-containing fuel that would be expected to promote fuel oxidation, recall that the MD engine runs were conducted at lower-temperature, lower-load conditions. The data suggest that the engine-load effect was more significant than fuel oxygen content in terms of the indicated specific HC and CO emissions.

Fuel-Conversion and Combustion Efficiencies. Fuel-conversion and combustion efficiencies are presented as a function of X_{O_2} in Figures 17 and 18, respectively. As shown in

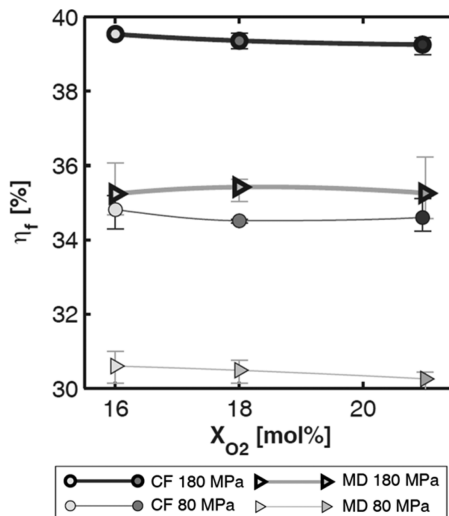


Figure 17. Fuel-conversion efficiency as a function of intake- O_2 mole fraction.

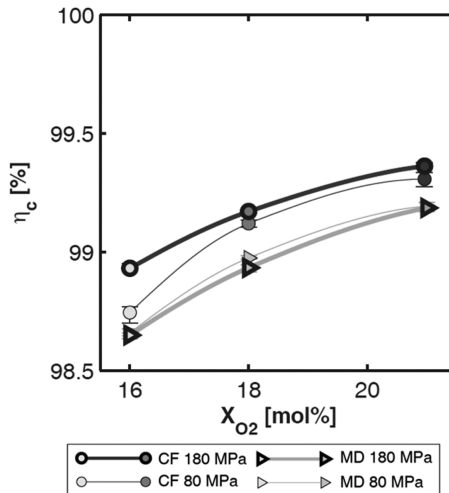


Figure 18. Combustion efficiency as a function of intake- O_2 mole fraction.

Figure 17, fuel-conversion efficiencies did not vary significantly with dilution but were higher at the higher 180-MPa injection pressure. This can be attributed to the combustion phasing effect described above (i.e., the closer-to-TDC heat release). Fuel-conversion efficiencies were lower for MD compared to CF, which can be explained by lower combustion efficiencies

(see Figure 18) resulting from incomplete oxidation as discussed above. Incomplete combustion (higher HC and CO emissions) at higher dilution levels also corresponds to the trends in combustion efficiency with respect to X_{O_2} in Figure 18.

4. SUMMARY AND CONCLUSIONS

An optically accessible heavy-duty diesel engine was used to investigate the impact of methyl decanoate (MD) on combustion and emissions, with a specific goal of determining whether soot-free LLFC could be achieved with the fuel. An ultralow sulfur diesel certification fuel (CF) was used as the baseline fuel, and experiments were conducted at two fuel-injection pressures and three levels of charge-gas dilution. In addition to conventional pressure-based and engine-out emissions measurements, exhaust LII, in-cylinder natural luminosity (NL), and in-cylinder chemiluminescence (CL) diagnostics were used to provide detailed insight into combustion processes.

The following observations and conclusions can be made for the engine-operating conditions investigated in this study:

(i) CF produced significant soot emissions that were effectively eliminated when the engine was fueled with MD. NL and CL measurements indicate that CF produced large amounts of in-cylinder soot that was not subsequently oxidized and thus left the engine to form exhaust PM. Using MD, soot-free LLFC was not achieved, with calculated equivalence ratios at the lift-off length in excess of ~ 3 . However, very little soot formation occurred in-cylinder, and soot that was formed was largely oxidized before exhaust-valve open.

(ii) Indicated specific NO_x emissions were lower for MD relative to CF at the higher 180-MPa injection pressure. At the lower 80-MPa injection pressure, however, MD NO_x emissions were higher. Results suggest that the higher adiabatic flame temperature of CF, combined with the higher load during CF fueling, lead to increased indicated specific NO_x emissions at the higher injection pressure. At the lower injection pressure, fuel atomization and charge-air mixing are more of a challenge, and thus the fuel-bound oxygen in MD may have played a more significant role, increasing indicated specific NO_x emissions relative to CF.

(iii) Indicated specific HC and CO emissions were higher with MD when compared to the corresponding CF cases. Although the oxygen content of MD would be expected to reduce HC and CO emissions by promoting oxidation, the influence of engine load on these emissions appeared to be more significant.

(iv) Calculated fuel-conversion and combustion efficiencies mirrored the HC and CO emissions results, with values lower for MD relative to CF.

While soot-free LLFC was not achieved using MD under the operating conditions of this study, it is possible that this nonsooting combustion mode could be achieved with MD under different engine operating conditions. Specifically, since higher fuel injection pressures decrease the equivalence ratio at the lift-off length, injection pressures beyond 180-MPa could achieve the lower than $\phi(H) \geq 2$ values needed for LLFC. Fuels with higher oxygen content than MD would also be expected to better promote LLFC.

Additional engine experiments and modeling efforts are underway to further investigate the impact of oxygenated fuels on mixing-controlled combustion in diesel engines. Data

obtained from this study will serve to guide those engine simulations in which MD is used as a biodiesel surrogate.

AUTHOR INFORMATION

Corresponding Author

*Address: School of Engineering, San Francisco State University, 1600 Holloway Avenue, SCI 123, San Francisco, CA 94132. Tel: 415-405-3486. E-mail: ascheng@sfu.edu.

Present Address

[§]Department of Mechanical and Aerospace Engineering, West Virginia University, P.O. Box 6106, Morgantown, West Virginia 26506, United States.

Notes

The authors declare no competing financial interest.

ACKNOWLEDGMENTS

This research was supported by the U.S. Department of Energy (DOE) and in-part by the DOE Visiting Faculty Program. The authors gratefully acknowledge DOE Office of Vehicle Technologies Program Manager Kevin Stork for long-term support of the optical-engine laboratory at Sandia. The research was conducted at the Combustion Research Facility, Sandia National Laboratories, Livermore, California. Sandia is a multiprogram laboratory operated by Sandia Corporation, a Lockheed Martin Company, for DOE's National Nuclear Security Administration under Contract DE-AC04-94AL85000.

REFERENCES

- (1) Pickett, L. M.; Siebers, D. L. Non-Sooting, Low Flame Temperature Mixing-Controlled DI Diesel Combustion. *SAE Trans.* **2004**, *113* (4), 614–630.
- (2) Pickett, L. M.; Siebers, D. L. Orifice Diameter Effects on Diesel Fuel Jet Flame Structure. *J. Eng. Gas Turbines Power* **2005**, *127* (1), 187–196.
- (3) Polonowski, C. J.; Mueller, C. J.; Gehrke, C. R.; Bazyn, T.; Martin, G. C.; Lillo, P. M. An Experimental Investigation of Low-Soot and Soot-Free Combustion Strategies in a Heavy-Duty, Single-Cylinder, Direct-Injection, Optical Diesel Engine. *SAE Int. J. Fuels Lubr.* **2012**, *5* (1), 51–77.
- (4) Fisher, E. M.; Pitz, W. J.; Curran, H. J.; Westbrook, C. K. Detailed Chemical Kinetic Mechanisms for Combustion of Oxygenated Fuels. *Proc. Combust. Inst.* **2000**, *28*, 1579–1586.
- (5) Gail, S.; Thomson, M. J.; Sarathy, S. M.; Syed, S. A.; Dagaut, P.; Diévert, P.; Marchese, A. J.; Dryer, F. L. A Wide-Ranging Kinetic Modeling Study of Methyl Butanoate Combustion. *Proc. Combust. Inst.* **2007**, *31* (1), 305–311.
- (6) Vaughn, T.; Hammill, M.; Harris, M.; Marchese, A. J. Ignition Delay of Bio-Ester Fuel Droplets; SAE Technical Paper 2006-01-3302; SAE International: Warrendale, PA, 2006.
- (7) Hakka, M. H.; Glaude, P.; Herbinet, O.; Battin-Leclerc, F. Experimental Study of the Oxidation of Large Surrogates for Diesel and Biodiesel Fuels. *Combust. Flame* **2009**, *156* (11), 2129–2144.
- (8) Brakora, J. L.; Ra, Y.; Reitz, R. D. Combustion Model for Biodiesel-Fueled Engine Simulations using Realistic Chemistry and Physical Properties. *SAE Int. J. Engines* **2011**, *4* (1), 931–947.
- (9) Herbinet, O.; Pitz, W. J.; Westbrook, C. K. Detailed Chemical Kinetic Oxidation Mechanism for a Biodiesel Surrogate. *Combust. Flame* **2008**, *154* (3), 507–528.
- (10) Herbinet, O.; Pitz, W. J.; Westbrook, C. K. Detailed Chemical Kinetic Mechanism for the Oxidation of Biodiesel Fuels Blend Surrogate. *Combust. Flame* **2010**, *157* (5), 893–908.
- (11) Seshadri, K.; Lu, T.; Herbinet, O.; Humer, S.; Niemann, U.; Pitz, W. J.; Seiser, R.; Law, C. K. Experimental and Kinetic Modeling Study of Extinction and Ignition of Methyl Decanoate in Laminar Non-Premixed Flows. *Proc. Combust. Inst.* **2009**, *32*, 1067–1074.
- (12) Diévert, P.; Won, S. H.; Dooley, S.; Dryer, F. L.; Ju, Y. A kinetic model for methyl decanoate combustion. *Combust. Flame* **2012**, *159*, 1793–1805.
- (13) Knothe, G. Designer Biodiesel: Optimizing Fatty Ester Composition to Improve Fuel Properties. *Energy Fuels* **2008**, *22*, 1358–1364.
- (14) Sarathy, S. M.; Thomson, M. J.; Pitz, W. J.; Lu, T. An Experimental and Kinetic Modeling Study of Methyl Decanoate Combustion. *Proc. Combust. Inst.* **2011**, *33*, 399–405.
- (15) Pyl, S. P.; Van Geem, K. M.; Puimège, P.; Sabbe, M. K.; Reyniers, M.-F.; Marin, G. B. A Comprehensive Study of Methyl Decanoate Pyrolysis. *Energy* **2012**, *42*, 146–160.
- (16) Li, Z.; Wang, W.; Huang, Z.; Oehlschlaeger, A. Autoignition of Methyl Decanoate, a Biodiesel Surrogate, under High-Pressure Exhaust Gas Recirculation Conditions. *Energy Fuels* **2012**, *26*, 4887–4895.
- (17) Liu, Y. C.; Farouk, T.; Savas, A. J.; Dryer, F. L.; Avedisian, C. T. On the spherically symmetrical combustion of methyl decanoate droplets and comparisons with detailed numerical modeling. *Combust. Flame* **2013**, *160*, 641–655.
- (18) Szybist, J. P.; Boehman, A. L.; Haworth, D. C.; Koga, H. Premixed Ignition Behavior of Alternative Diesel Fuel-Relevant Compounds in a Motored Engine Experiment. *Combust. Flame* **2007**, *149*, 112–128.
- (19) Fisher, B. T.; Mueller, C. J. Liquid-Phase Penetration under Unsteady In-Cylinder Conditions: Soy- and Cuphea-Derived Biodiesel Fuels Versus Conventional Diesel. *Energy Fuels* **2010**, *24*, 5163–5180.
- (20) Wang, X.; Yao, M.; Li, S.; Gu, J. *Experimental and Modeling Study of Biodiesel Surrogates Combustion in a CI Engine*; SAE Technical Paper 2013-01-1130; SAE International: Warrendale, PA, 2013.
- (21) Manin, J.; Skeen, S.; Picket, L.; Kurtz, E.; Anderson, J. E. Effects of Oxygenated Fuels on Combustion and Soot Formation/Oxidation Processes. *SAE Int. J. Fuels Lubr.* **2014**, *7* (3), 704–717.
- (22) Fisher, B. T.; Mueller, C. J. Liquid Penetration Length of Heptamethylnonane and Trimethylpentane under Unsteady in-Cylinder Conditions. *Fuel* **2010**, *89* (10), 2673–2696.
- (23) Kempenaar, J. G.; Mueller, C. J.; Shollenberger, K. A. *An Instrument for Measuring Orifice-Specific Fuel-Injection Rate from a Multi-Orifice Nozzle (FEDSM 2008-55047)*; presented at ASME Fluids Engineering Division Summer Meeting, Jacksonville, FL, August 10–14, 2008.
- (24) Axelsson, B.; Witze, P. O. *Qualitative Laser-Induced Incandescence Measurements of Particulate Emissions During Transient Operation of a TDI Diesel Engine*; SAE Technical Paper 2001-01-3574; SAE International: Warrendale, PA, 2001.
- (25) Cheng, A. S.; Upatnieks, A.; Mueller, C. J. Investigation of Fuel Effects on Dilute, Mixing-Controlled Combustion in and Optical Direct-Injection Diesel Engine. *Energy Fuels* **2007**, *21*, 1989–2002.
- (26) NIST Chemistry WebBook (NIST Standard Reference Database Number 69); <http://webbook.nist.gov/chemistry/> (accessed Aug 13, 2014).
- (27) Mueller, C. J.; Cannella, W. J.; Bruno, T. J.; Bunting, B.; Dettman, H.; Franz, J.; Huber, M. L.; Natarajan, M.; Pitz, W. J.; Ratcliff, M. A.; Wright, K. Methodology for Formulating Diesel Surrogate Fuels with Accurate Compositional, Ignition-Quality, and Volatility Characteristics. *Energy Fuels* **2012**, *26* (6): 3284–3303.
- (28) Dec, J. E.; Espey, C. Chemiluminescence Imaging of Autoignition in a DI Diesel Engine. *SAE Trans.* **1998**, *107* (3), 2230–2254.
- (29) Mueller, C. J.; Martin, G. C. Effects of Oxygenated Compounds on Combustion and Soot Evolution in a DI Diesel Engine: Broadband Natural Luminosity Imaging. *SAE Trans.* **2002**, *111* (4), 518–537.
- (30) Higgins, B.; Siebers, D. Measurement of the Flame Lift-Off Location on D.I. Diesel Sprays Using OH Chemiluminescence. *SAE Trans.* **2001**, *110* (3), 739–753.
- (31) Pickett, L. M.; Siebers, D. L.; Idicheria, C. A. Relationship between Ignition Processes and the Lift-Off Length of Diesel Fuel Jets. *SAE Trans.* **2005**, *114* (3), 1714–1731.

- (32) Mueller, C. J.; Boehman, A. L.; Martin, G. C. An Experimental Investigation of the Origin of Increased NO_x Emissions When Fueling a Heavy-Duty Compression-Ignition Engine with Soy Biodiesel. *SAE Int. J. Fuels Lubr.* **2009**, *2* (1), 789–816.
- (33) Naber, J. D.; Siebers, D. L. Effects of Gas Density and Vaporization on Penetration and Dispersion of Diesel Sprays. *SAE Trans.* **1996**, *105* (3), 82–111.
- (34) Pickett, L. M.; Siebers, D. L. Soot Formation in Diesel Fuel Jets near the Lift-Off Length. *Int. J. Engine Res.* **2006**, *7* (2), 103–130.
- (35) Pickett, L. M.; Manin, J.; Genzale, C. L.; Siebers, D. L.; Musculus, M. P. B.; Idicheria, C. A. Relationship between Diesel Fuel Spray Vapor Penetration/Dispersion and Local Fuel Mixture Fraction. *SAE Int. J. Engines* **2011**, *4* (1), 764–799.
- (36) Dumitrescu, C. E.; Polonowski, C.; Fisher, B. T.; Cheng, A. S.; Lilik, G. K.; Mueller, C. J. An Experimental Study of Diesel-Fuel Property Effects on Mixing-Controlled Combustion in a Heavy-Duty Optical CI Engine. *SAE Int. J. Fuels Lubr.* **2014**, *7* (1), 65–81.
- (37) Musculus, M. P. B. Effects of the in-Cylinder Environment on Diffusion Flame Lift-Off in a DI Diesel Engine. *SAE Trans.* **2003**, *112* (3), 314–337.
- (38) *A Comprehensive Analysis of Biodiesel Impacts on Exhaust Emissions: Draft Technical Report*; report no. EPA420-P-02-001; U.S. Environmental Protection Agency: Washington, D.C., 2002.
- (39) Cheng, A. S.; Upatnieks, A.; Mueller, C. J. Investigation of the impact of biodiesel fuelling on NO_x emissions using an optical direct injection diesel engine. *Int. J. Engine Res.* **7** (4): 297–318.
- (40) Gysel, N.; Karavalakis, G.; Durbin, T.; Schmitz, D.; Cho, A. *Emissions and Redox Activity of Biodiesel Blends Obtained from Different Feedstocks from a Heavy-Duty Vehicle Equipped with DPF/SCR Aftertreatment and a Heavy-Duty Vehicle without Control Aftertreatment*; SAE Technical Paper 2014-01-1400; SAE International: Warrendale, PA, 2014.
- (41) Siebers, D.; Higgins, B.; Pickett, L. *Flame Lift on Direct-Injection Diesel Fuel Jets: Oxygen Concentration Effects*; SAE Technical Paper 2002-01-0890; SAE International: Warrendale, PA, 2002.
- (42) Dec, J. Advanced Compression-Ignition Engines – Understanding the In-Cylinder Processes. *Proc. Combust. Inst.* **2009**, *32*, 2727–2742.
- (43) Hoffman, S. R.; Abraham, J. A Comparative Study of *n*-Heptane, Methyl Decanoate, and Dimethyl Ether Combustion Characteristics Under Homogeneous-Charge Compression-Ignition Engine Conditions. *Fuel* **2009**, *88*, 1099–1108.
- (44) Fisher, E. M.; Pitz, W. J.; Curran, H. J.; Westbrook, C. K. Detailed Chemical Kinetic Mechanisms for Combustion of Oxygenated Fuels. *Proc. Combust. Inst.* **2000**, *28*, 1579–1586.